The activation strain model of chemical reactivity

Willem-Jan van Zeist and F. Matthias Bickelhaupt*

Received 22nd December 2009, Accepted 4th May 2010
First published as an Advance Article on the web 20th May 2010
DOI: 10.1039/b926828f

Herein, we provide an account of the activation strain model of chemical reactivity and its recent applications. In this model, the potential energy surface $\Delta E(\zeta)$ along the reaction coordinate ζ is decomposed into the strain $\Delta E_{\text{strain}}(\zeta)$ of the increasingly deformed reactants plus the interaction $\Delta E_{\text{int}}(\zeta)$ between these deformed reactants, *i.e.*, $\Delta E(\zeta) = \Delta E_{\text{strain}}(\zeta) + \Delta E_{\text{int}}(\zeta)$. The purpose of this fragment-based approach is to arrive at a qualitative understanding, based on accurate calculations, of the trends in activation barriers and transition-state geometries (*e.g.*, early or late along the reaction coordinate) in terms of the reactants' properties. The usage of the activation strain model is illustrated by a number of concrete applications, by us and others, in the fields of catalysis and organic chemistry.

1. Introduction

Chemistry is about structure, properties and especially reactions of molecules. A core task of chemistry is the design and utilization of new molecules and the synthetic routes towards these molecules. A prerequisite for a more rational design of efficient reactions, *i.e.*, with low barriers for the desired pathway (but not for side reactions!) is, therefore, a detailed understanding of the factors that control the relative heights of reaction barriers of the competing pathways.

Department of Theoretical Chemistry and Amsterdam Center for Multiscale Modeling, VU University, De Boelelaan 1083, NL-1081 HV, Amsterdam, The Netherlands. E-mail: fm.bickelhaupt@few.vu.nl; Fax: +31-20-5987629

Nevertheless, this aspect of chemistry is still largely an empirical business, based on trial and error. This is so not only in experimental but also in computational chemistry, despite the many pioneering contributions that furthered particular areas of reactivity. Examples are the Woodward–Hoffmann rules in molecular orbital (MO) theory,[1-3] elaborated upon by Dewar,[4] the concept of charge *versus* orbital control,[5] the valence bond (VB) curve crossing model,[6] or Marcus theory[7] and extensions thereof.[8]

The activation strain model of chemical reactivity provides the ingredients required for a thorough understanding of chemical reactivity and trends therein in terms of the properties of the reactants. In the first place, it relates the height of the activation energy to the rigidity of the reactants and the geometrical

Willem-Jan van Zeist

Willem-Jan van Zeist studied chemistry at VU University Amsterdam (2001–2006) where he received his M.Sc. degree in theoretical chemistry. He is currently finishing his Ph.D. under the guidance of Matthias Bickelhaupt. His research focuses on the application of the activation strain model on various chemical reactions, with an emphasis on metal-mediated bond activation. Willem-Jan van Zeist is the author of the PyFrag program which helped him and others to conveniently carry out and interpret activation strain analyses for large numbers of reactions.

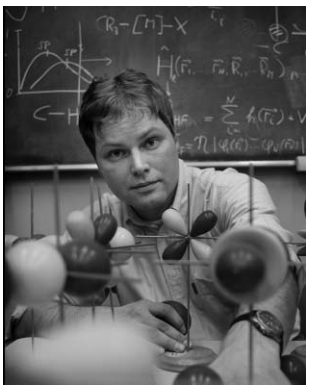

Matthias Bickelhaupt

Matthias Bickelhaupt is full professor and head of the Department of Theoretical Chemistry at VU University Amsterdam. He received his M.Sc. degree in theoretical chemistry with Evert Jan Baerends (VU University Amsterdam), his Ph.D. in mass spectrometry and theoretical chemistry with Nico Nibbering (University of Amsterdam) and Evert Jan Baerends, and was a postdoctoral associate in the groups of Paul von Ragué Schleyer (Erlangen, Germany), Tom Ziegler (Calgary, Canada) and Roald Hoffmann (Cornell University, USA). In 1997 he was appointed assistant professor in the lab of Gernot Frenking (Marburg, Germany) and obtained tenure in 1999 at VU University in Amsterdam. He is the winner of various scholarships and prizes, including selection as professor at the prestigious Amsterdam University College (AUC) in 2009 and the 2002 VICI award of the Netherlands Organization of Scientific Research (NWO). His research interests cover a range of topics in the fields of chemical bonding and structure, biochemistry, reactivity, and catalysis.

deformation that is associated with (and characteristic for) the reaction pathway under consideration. This aspect of geometrical distortion shows up in the destabilizing strain energy. The second quantity in this model is related to the bonding capabilities and mutual interaction between the increasingly deformed reactants along the same pathway (*vide infra*).

In this emerging area paper, we will give an overview of the activation strain model and various applications, by us and others, in the fields of catalysis and organic chemistry. We cover not only metal-mediated bond activation (oxidative addition) and ligand effects thereon, but also nucleophilic substitution and pericyclic reactions.

2. Activation strain model

As already indicated briefly above, the activation strain model is a fragment-based approach to understanding chemical reactions and the associated barriers.[9] The starting point is the two separate reactants, which approach from infinity and begin to interact and deform each other. In this model, the activation energy $\Delta E^{\ddagger}$ of the transition state (TS) is decomposed into the strain energy $\Delta E^{\ddagger}_{\text{strain}}$ and the interaction energy $\Delta E^{\ddagger}_{\text{int}}$ (see eqn (1) and Fig. 1):

$$\Delta E^{\ddagger} = \Delta E^{\ddagger}_{\text{strain}} + \Delta E^{\ddagger}_{\text{int}} \quad (1)$$

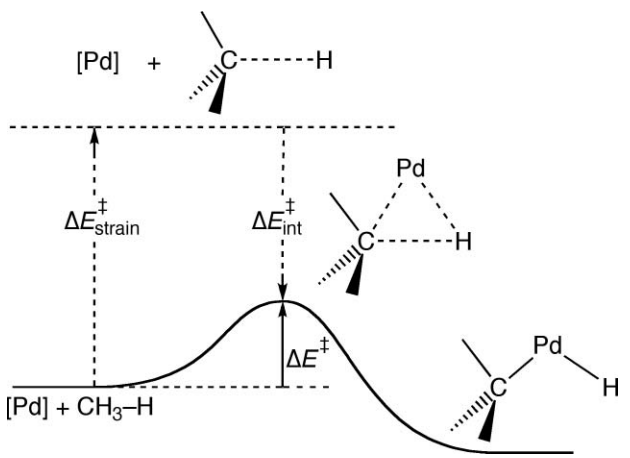

Fig. 1 Illustration of the activation strain model using oxidative insertion of a [Pd] complex into the methane C–H bond.

The activation strain $\Delta E^{\ddagger}_{\text{strain}}$ is the energy associated with deforming the reactants from their equilibrium geometry into the geometry they acquire in the activated complex. It can be divided into a contribution stemming from each of the reactants, *e.g.*, catalyst and substrate strain in the case of catalytic bond activation. The TS interaction $\Delta E^{\ddagger}_{\text{int}}$ is the actual interaction energy between the deformed reactants in the transition state.

The model can be extended to incorporate the entire reaction path.[9–11] The decomposition of the energy $\Delta E(\zeta)$ into strain $\Delta E_{\text{strain}}(\zeta)$ and interaction $\Delta E_{\text{int}}(\zeta)$ is carried out along the reaction coordinate ζ, *i.e.*, from reactants *via* TS to products. The reaction coordinate, ζ, is usually obtained as the intrinsic reaction coordinate (IRC) from a steepest-descent calculation. This reaction coordinate may then be projected onto a critical geometrical parameter, such as the bond that is broken during a bond activation process.[13]

The values of $\Delta E^{\ddagger}_{\text{strain}}$ and $\Delta E^{\ddagger}_{\text{int}}$ at the TS must be interpreted with great care, since the optimized TS structure is the result of a balance of the components $\Delta E_{\text{strain}}(\zeta)$ and $\Delta E_{\text{int}}(\zeta)$. Along the reaction coordinate, the strain $\Delta E_{\text{strain}}(\zeta)$ increases, in general, because the substrate becomes increasingly deformed. At the same time, the interaction $\Delta E_{\text{int}}(\zeta)$ becomes more stabilizing in most cases. The net result is the total energy profile $\Delta E(\zeta)$ which achieves its maximum (*i.e.*, the TS) at the point along the reaction coordinate where $\mathrm{d}\Delta E_{\text{strain}}(\zeta)/\mathrm{d}\zeta = -\mathrm{d}\Delta E_{\text{int}}(\zeta)/\mathrm{d}\zeta$.

This highlights the importance of taking into account the behavior of the two components along the reaction coordinate, especially their slopes. A single-point analysis at the TS, only, yields values that can be misleading, as can be seen from the activation strain diagrams in Fig. 2. For example, going from reaction A to reaction B in Fig. 2a causes the barrier to decrease. A single-point analysis at the respective TSs indicates that this is due to a lower activation strain, not because of a more stabilizing TS interaction. This suggests that the mutual bonding capability of the reactants in reaction B is reduced but that the barrier is nevertheless lower because of a lower rigidity or a less distortive character of the reaction as compared to reaction A. However, the more complete analysis in Fig. 2a shows that this is obviously incorrect. The

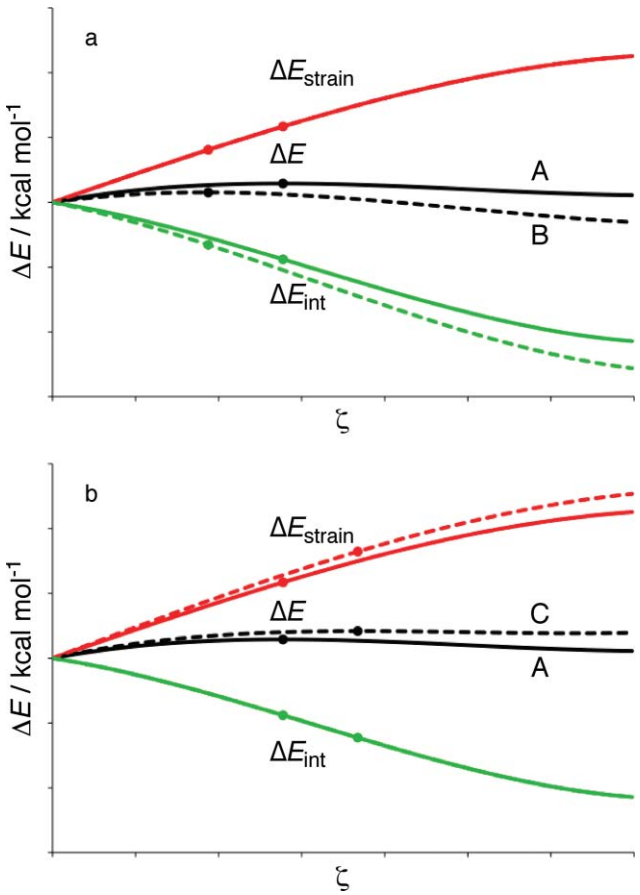

Fig. 2 Schematic illustration of activation strain analyses for arbitrary reactions A, B and C. (a) From reaction A to B, the interaction energy becomes more stabilizing, which lowers the TS (indicated by a dot) and shifts it towards the educt side, at the left. (b) From reaction A to C, the strain energy becomes more destabilizing, which raises the TS and shifts it towards the product side, at the right.

interaction ΔE_{int} of reaction B is *more stabilizing at any given point along the reaction coordinate* than ΔE_{int} of reaction A. The fact that this seems to be reversed in the single-point analyses is due to the fact that the TS structures of A and B occur at different locations along the reaction path. An equivalent reasoning also applies when going from reaction A to reaction C (Fig. 2b), where the interaction energy is similar along the entire path, an observation that would be missed when looking at the TSs only.

Note that in the activation strain diagrams in Fig. 2, all energy curves start, on the reactant side, at zero kcal mol^{-1}. However, reactions often proceed from a reactant complex that is formed prior to traversing the transition state. Such a precursor complex is then conveniently used as the starting point for the activation-strain analysis. Therefore, in practice, the energy curves of an activation strain analysis start at a point in the diagram where the reaction coordinate ζ is already slightly larger than zero (reactant complex formation) and the reactants do already (weakly) interact and deform each other, *i.e.*, $\Delta E(\zeta)$, $\Delta E_{strain}(\zeta)$, and $\Delta E_{int}(\zeta)$ may already slightly deviate from zero (see figures later on).

The interaction ΔE_{int} between the deformed reactants can be further analyzed in the conceptual framework provided by the Kohn–Sham molecular orbital model.[14,15] Thus, $\Delta E_{int}(\zeta)$ is further decomposed into three physically meaningful terms (eqn (2)) using a quantitative energy decomposition scheme developed by Ziegler and Rauk.[14,16]

$$\Delta E_{int}(\zeta) = \Delta V_{elst}(\zeta) + \Delta E_{Pauli}(\zeta) + \Delta E_{oi}(\zeta) \quad (2)$$

These three terms allow a thorough assessment of the interaction between the deformed reactants. The term ΔV_{elst} corresponds to the classical electrostatic interaction between the unperturbed charge distributions of the deformed reactants and is usually attractive. The Pauli repulsion ΔE_{Pauli} comprises the destabilizing interactions between occupied orbitals and is responsible for the steric repulsion. The orbital interaction ΔE_{oi} accounts for charge transfer (interaction between occupied orbitals on one moiety with unoccupied orbitals of the other, including the HOMO–LUMO interactions) and polarization (empty–occupied orbital mixing on one fragment due to the presence of another fragment).

The reaction path to be analyzed can be found in a number of ways, the most accurate being the intrinsic reaction coordinate (IRC) method.[17–20] The IRC methods yields the minimum energy path connecting reactants and products *via* the paths of steepest descent from the associated transition state. After obtaining the reaction profile, any quantum mechanical program package is able to perform an activation strain analysis. However, the quantitative energy decomposition scheme as described above has only been implemented in the Amsterdam Density Functional program package (ADF). For ADF, the PyFrag program has been developed, which acts as a wrap-around for ADF and streamlines performing the activation strain analysis of IRC calculations.[21]

In addition to studying reactions that proceed *via* energy barriers, the activation strain model can also be applied to simple, barrier-free bond formation reactions: A + B → A–B. The stability and length of the emerging A–B bond are again a result of an interplay between stabilizing and destabilizing forces, very similar to the situation described above for the energy of the TS and its position along the reaction coordinate. Thus, the same precaution should be taken if one attempts to reveal the origin of the strength and length of bonds in stable molecules based solely on the basis of a single-point analysis at the equilibrium geometry. It is always more complete (and sometimes even crucial) to carry out the analysis along the "reaction coordinate", *i.e.*, as a function of the bond distance under consideration.[22]

The concepts of strain and interaction that feature in the activation strain model may *seem* to be reminiscent of concepts in other reactivity models. For example, in VB theory, the reaction profile is conceived as resulting from distorted diabatic reactant and product states that interact and mix near the TS at which their state energy curves cross.[6] Note however that in VB theory (and also, *e.g.*, in Marcus theory[7]) the concepts of distortion and interaction refer to the entire reaction system, either from the point of view of the reactants (reactant state) or products (product state). There is thus no straightforward relationship with the strain and interaction in the activation strain model in which these concepts refer to the individual reactants that become increasingly distorted and also interact more and more strongly as the reaction progresses toward the products.

Finally, the activation strain model has evolved from studying bimolecular reactions. It can however also be applied to unimolecular processes, for example, the internal rotation of ethane[23] and biphenyl.[24] Note that, in the case of unimolecular reactions, one has to make an explicit choice of fragments within the reorganizing species (*e.g.*, the two methyl fragments that rotate with respect to each other in ethane) whereas for bimolecular reactions these fragments are by default the two reactants.

3. Bond activation

The activation strain model has been thoroughly applied to a well-known class of processes involving oxidative addition in catalytic bond activation (see Scheme 1 and Fig. 1).[25–27] The catalytically active species in these reactions are generally coordination complexes of palladium or other transition metals. This process is an efficient tool for selectively converting simple educts, *via* C–C bond formation, into more complex compounds, and is therefore of major importance for synthetic chemistry. In previous studies, our group has used the activation strain model to gain insight into how variations in the metal, the ligands and the substrates affect the activation barriers of the different oxidative addition reactions.[28–35]

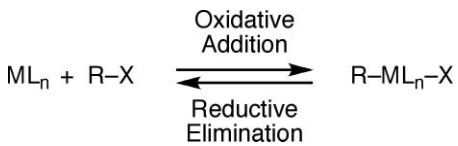

Scheme 1 Oxidative addition and reductive elimination.

Oxidative insertion is essentially a (metal-mediated) bond-breaking process, where the strength of the bond is of obvious importance. The energy related to the bond-breaking is reflected by the strain term of the substrate. The bond-breaking process is facilitated by a back-donation interaction of metal d orbitals into the empty σ* antibonding orbital of the activated bond in the substrate (see Scheme 2). In the following subsections, some examples are given of activation strain analyses on various oxidative insertion processes.

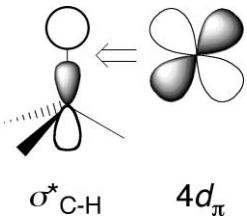

Scheme 2 Schematic representation of the back-donation in the oxidative insertion of bare palladium into the methane C–H bond.

3.1. Substrate effects on bond activation

An interesting example of strain effects on the substrate is insertion into the C–C bond in cyclopropane (see Scheme 3).[12] Compared to the C–C bond in ethane, one may expect a relatively easy insertion process due to the weak C–C bond in the highly strained ring system. Indeed, this insertion proceeds without any barrier (except for a small barrier upon breaking free from the reactant complex prior to the insertion). This is a radical change compared to the 18 kcal mol^{-1} barrier for the insertion into the ethane C–C bond. The activation strain model can straightforwardly show that this decrease in bond strength lowers the insertion barrier because of the lower strain energy term.

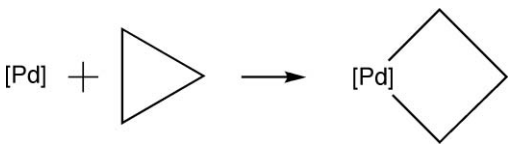

Scheme 3 Oxidative insertion of palladium into the strained C–C bond in cyclopropane.

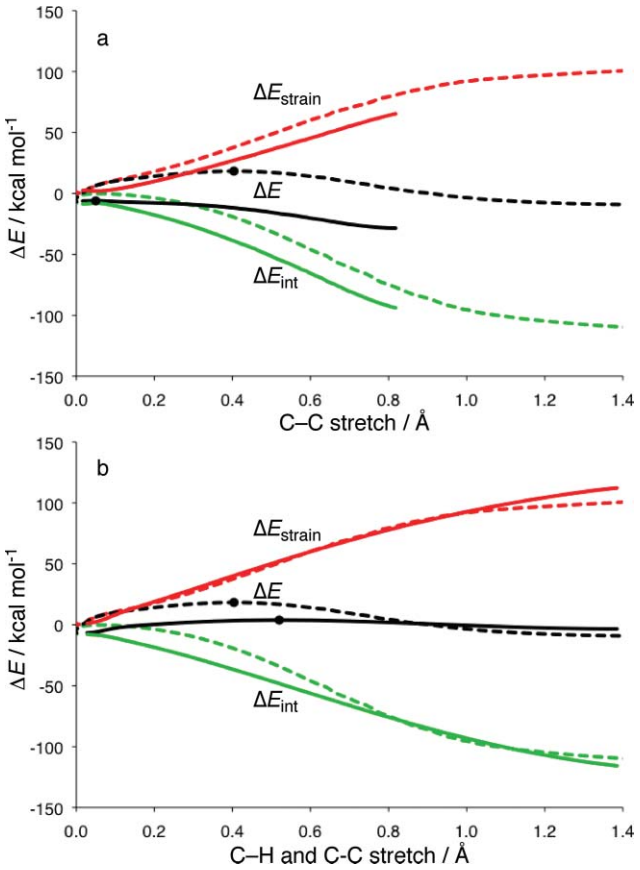

Fig. 3 Activation strain analyses for oxidative insertion of Pd into (a) the ethane C–C (dashed lines) and cyclopropane C–C bond (solid lines); (b) the ethane C–C (dashed lines) and methane C–H bond (solid lines).[12]

However, activation strain analyses reveal more features responsible for the lower barrier. Besides the decrease in the strain energy, it appears that the strained system also allows for easier access of the palladium to the C–C bond. In the ethane oxidative insertion, the hydrogens on the methyl groups have to bend away in order to allow contact of the palladium with the C–C bond. The interaction with the bond is thus greatly reduced due to steric shielding of the methyl groups. In cyclopropane this bending away of the hydrogens is already built into the geometry of the substrate, thus allowing for stronger interaction early along the reaction path. Both effects can be clearly recognized in Fig. 3a: both the strain and interaction terms are stabilized for oxidative insertion into cyclopropane (solid lines) as compared to the situation for ethane (dashed lines).

It is interesting to compare this with the corresponding oxidative insertion into the methane C–H bond, shown in Fig. 3b. The methane C–H activation barrier is some 14 kcal mol^{-1} lower despite the fact that this bond is much stronger than the C–C bond. The reason for the low C–H activation barrier is similar to that for the C–C bond in cyclopropane: there is very little steric shielding on the side of the hydrogen, so interaction with the C–H bond proceeds easily, right from the beginning. In contrast, the C–C bond is shielded on both ends by the methyl C–H bonds which prevent the palladium atom to approach and "electronically touch" the C–C bond for some time.[36,37] Only after the C–C bond has been sufficiently elongated and the methyl groups have tilted away, is there room for the metal atom to come closer and build up overlap between its d orbitals and the C–C σ* acceptor orbital. The initial delay in metal–substrate interaction ΔE_{int} in the case of the ethane C–C activation can be clearly seen in Fig. 3b: compare green dashed (C–C) and green solid (C–H) curves.

In other work, Legault *et al.* used the activation strain model to analyze regioselectiviy in palladium-catalyzed cross-coupling reactions with heterocycles bearing multiple identical halogens.[38] Their results show that the selectivity is determined by both the strength of the carbon–halogen bond (which depends on its position in the heterocycle) and the nature of the interacting LUMO of the heterocycle. These properties are directly related to the strain and interaction energy terms. Previously, we have found similar causal relationships. The low reaction barrier, for example, for C–Cl as compared to C–H bond activation by palladium, is explained straightforwardly by the lower C–Cl bond strength, which manifests itself in a less destabilizing ΔE_{strain} curve.[12]

Good correlations between activation strain and reaction barrier were also found by Gorelsky *et al.* for the concerted metalation–deprotonation mechanism in palladium-catalyzed direct arylation,[39] and by Ess *et al.* for iridium-induced activation of methane and benzene C–H bonds, assisted by acetate ligands.[40]

Ariafard *et al.* used an activation strain analysis to shed light on the differences in activation barriers of aryl and alkyl halides.[41] They showed that the former have lower barriers because the availability of low lying π*-orbitals leads to a more favorable interaction energy ΔE_{int}.

3.2 Ligand effects on bond activation

Ligands obviously are of great importance for determining the activity and selectivity of catalysts in general and catalytic bond activations, in particular. The effect of anion assistance on catalytic bond activation has been studied with the activation strain model by comparing the oxidative addition reaction of Pd (no assistance) to that of $PdCl^-$ ("anion assisted").[12,29,31] Introducing the chloride ligand on palladium lowers activation barriers and increases the exothermicity of all model reactions. This is nearly exclusively caused by a more favorable interaction curve ΔE_{int} in the case of the anion-assisted process, as illustrated for C–H bond activation in Fig. 4a. The strain energy ΔE_{strain} depends mainly on the strength of the bond that is activated and is hardly affected by anion assistance. Note that the steeper descent of the more stabilizing ΔE_{int} curve, in the case of $PdCl^-$, not only lowers the energy of the TS but also shifts it to an earlier position along the reaction coordinate.

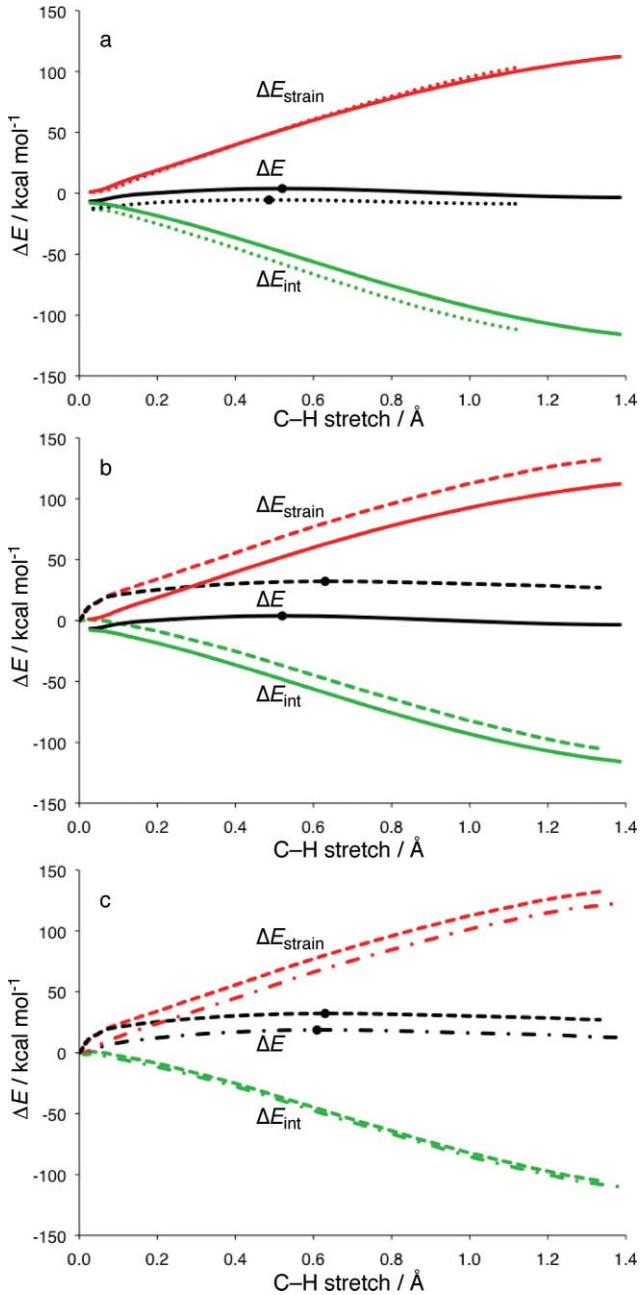

Fig. 4 Activation strain analyses of methane C–H activation by: (a) Pd (solid curves) and $PdCl^-$ (dotted), (b) by Pd (solid) and $Pd(PH_3)_2$ (dashed), and (c) $Pd(PH_3)_2$ (dashed) $Pd[PH_2(CH_2)_2PH_2]$ (dash-dotted).

Phosphine ligands play a central role in metal-mediated catalytic processes. The so-called "bite angle" (the ligand–metal–ligand angle, see Scheme 4, left) has been identified as a key factor that determines the catalytic activity of metal complexes involving chelating bidentate ligands. Recently, we have investigated the bite angle effect with the activation strain model.[35]

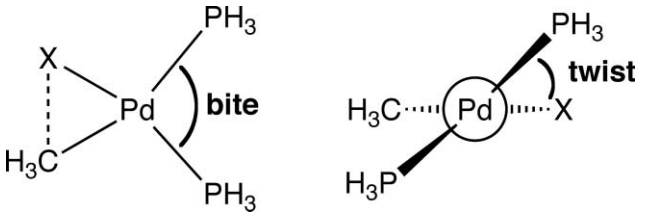

Scheme 4 Bite and twist angles.

The common idea is that by bending the metal complex away from linearity, the ligand lone pairs push the metal d orbital up in energy, thus increasing their electron donor capability and strengthening the HOMO–LUMO interactions with the substrate's σ^* acceptor orbital. The more stabilizing interaction between catalyst and substrate is held responsible for the observed lower activation energy for metal complexes with smaller bite angles.

Activation strain analyses show that this idea of an electronic bite-angle effect is not correct.[35] The bite angle effect rather has a geometrical or steric nature. This is illustrated by Fig. 4b and 4c. Fig. 4b compares methane C–H bond activation by Pd (solid curves) and $Pd(PH_3)_2$ (dashed curves). As can be seen, the introduction of phosphine ligands raises the barrier, that is, it makes the catalyst less active. This appears to come from both increased strain ΔE_{strain} and less stabilizing interaction ΔE_{int}. Closer inspection reveals that both effects have a common origin. The phosphine ligands experience steric (Pauli) repulsion with the substrate, and this repulsion increases as the oxidative-addition reaction proceeds. This causes the interaction to become less favorable. At the same time, part of the steric repulsion is relieved by the phosphine ligands bending away from the substrate. This shows up in an additional amount of strain, building up at the beginning of the reaction path. This stems from the catalyst's bending deformation (we recall that the total strain energy can be decomposed into a contribution stemming from the catalyst and one stemming from the substrate; see ref. 35). In particular, in the early stages of the reaction, steric repulsion between the catalyst's ligands and the substrate is also relieved by adopting a twist angle larger than 0° (see Scheme 4, right).

The catalyst's bending strain can be deleted from the reaction energy profile by "building it into the catalyst", right from the beginning. This is what happens when we introduce a short bridge that pulls together the two phosphine centers in a bidentate ligand, as can be seen in Fig. 4c. Here, methane C–H activation by $Pd(PH_3)_2$ (dashed curves) is compared with that by $Pd[PH_2(CH_2)_2PH_2]$ (dash-dotted curves) in which the phosphines are connected *via* a dimethylene bridge (see also Fig. 5). In the

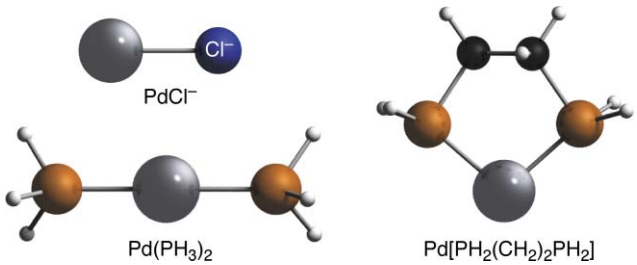

Fig. 5 Model catalysts used to study ligand effects.

reaction of $Pd[PH_2(CH_2)_2PH_2]$, the bending strain no longer builds up during the reaction. This is reflected by a corresponding drop in the strain curve and thus a lowering of the activation barrier in ΔE. Note that the interaction curve ΔE_{int} is stabilized only marginally in the reaction of $Pd[PH_2(CH_2)_2PH_2]$.

Fazeali *et al.*[42] have shown that $Pd(PCl_3)_2$ has a softer bending potential than $Pd(PH_3)_2$. This translates into less strain ΔE_{strain} along the reaction path of the $Pd(PCl_3)_2$-induced bond activation and, therefore, a lower activation energy. Interestingly, the fact that strain is a less important factor in the reactions involving the trichloro-substituted phosphine ligands makes electronic factors (*i.e.*, changes in interaction ΔE_{int}) become more important, for example, if one goes from bond activation by $Pd(PCl_3)_2$ to that by the chelate complex $Pd[PCl_2(CH_2)_2PCl_2]$.

Ariafard and Yates have used activation strain analyses for studying reductive elimination, the reverse reaction of oxidative addition (see Scheme 1).[43] They found that reductive elimination of R–R from $Pd(PH_3)_2R_2$ is promoted by the concomitant release of bending strain in the evolving $Pd(PH_3)_2$ complex, and this effect becomes larger for sterically more demanding phosphine ligands. For comparison, such a promoting factor was found to be absent in the corresponding reductive elimination of R–R from $PdPH_3R_2$.

3.3 Metal variation

Recently, we have investigated how C–X bond activation by the group-11 transition-metal cations Cu^+, Ag^+ and Au^+ differs from that by the isoelectronic Pd atom.[44] Oxidative insertion of the second-row transition-metal species Ag^+ and Pd was found, for a given bond, to yield the highest overall reaction barriers. It is tempting, but incorrect, to attribute the similar barrier heights for Ag^+ and Pd to a presumed similarity in the metal–substrate interaction of these isolelectronic second-row transition metal species. In fact, the difference in net charge translates into completely different bonding capabilities of the three metal cations on one hand and the neutral palladium on the other hand. The former have shallower interaction curves because of favorable substrate→metal n*s* donation in early stages of the reaction and reduced metal→substrate backdonation from the (n–1)*d* AOs at later stages of the reaction. As can be seen in the activation-strain diagrams of Fig. 6, this causes the transition state (TS) to shift towards the product side where the strain curves are more destabilizing. The final position along the reaction coordinate depends in a subtle manner on the shape and balance between $\Delta E_{strain}(\zeta)$ and $\Delta E_{int}(\zeta)$, and may yield not only a stabilized (Cu^+, Au^+; see Fig. 6a and 6b) but also a destabilized TS, as in the case of Ag^+ (see Fig. 6c)

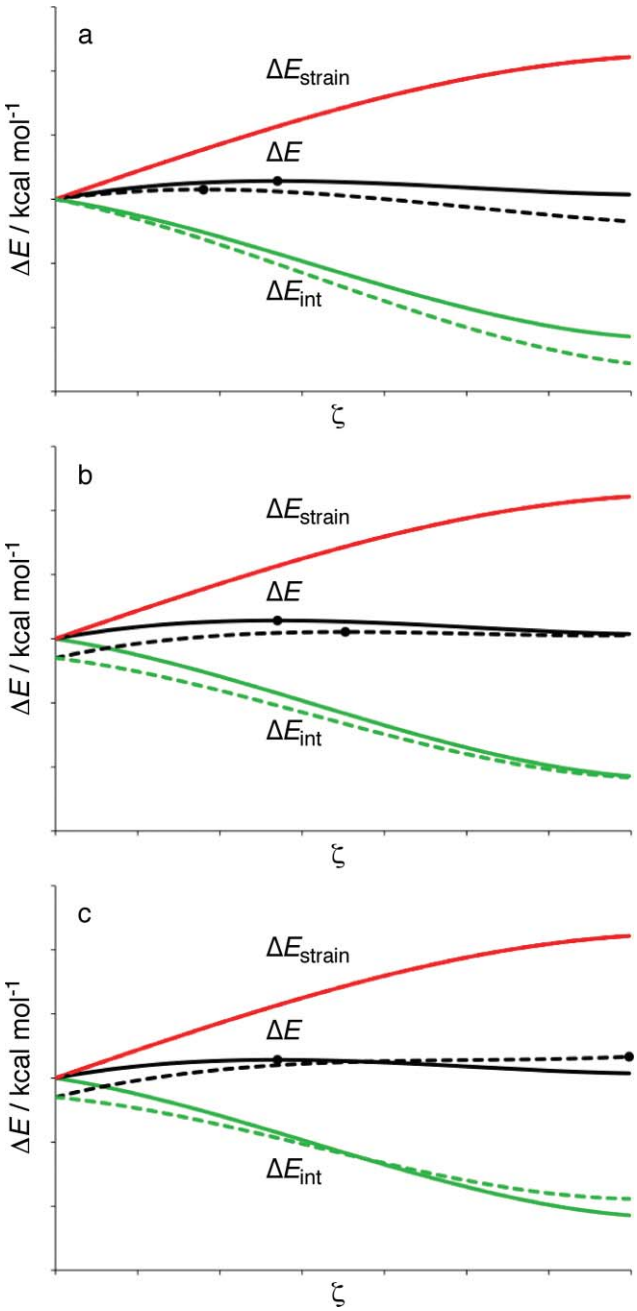

Fig. 6 Schematic activation strain diagrams for illustrating how the reaction profile ΔE is affected by: (a) stabilizing the ΔE_{int} curve at the product side; (b) stabilizing the ΔE_{int} curve at the reactant side; (c) stabilizing the ΔE_{int} curve at the reactant side and destabilizing it at the product side. Note that the strain curve ΔE_{strain} is identical in a–c, which corresponds to a variation of the metal species inserting into the same bond.[44]

An earlier study addressed the question why transition (or d-block) metals, such as Pd, are better agents for oxidative insertion into C–X bonds than group-12 transition metals (Zn, Cd) and main group metals (Be, Mg, Ca).[32] Activation strain analyses show that this can be mainly ascribed to palladium's excellent electron-donating and accepting capabilities associated with the high-energy 4*d* HOMO and low-energy 5*s* LUMO. Together, this

causes a more stabilizing palladium–substrate interaction $\Delta E_{int}(\zeta)$ at any point along the reaction coordinate.

3.4 Competition with S_N2 substitution and solvent effects

Oxidative addition of a C–X bond may proceed not only *via* direct oxidative insertion (OxIn) but also *via* a competing pathway of nucleophilic substitution, in particular when X is an electronegative group (see Scheme 5). A case in point is the activation of the carbon–halogen bonds in halomethanes which has been investigated using the activation strain model.[12,31,33,34] The difference between the mechanisms is important since it corresponds to a change in stereochemistry at the carbon atom involved, namely, from retention of configuration for OxIn to inversion of configuration for S_N2. This is relevant in syntheses involving substrates that bear a chiral carbon atom (*e.g.*, RR′R″C*–X).

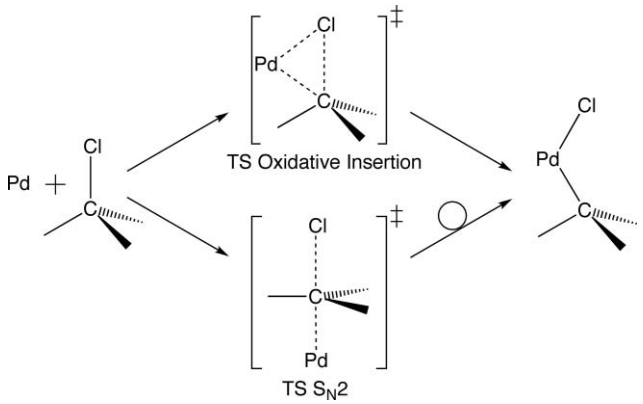

Scheme 5 Oxidative insertion (OxIn) and S_N2 substitution pathways for C–Cl bond activation.

In the gas phase, the reaction barrier for oxidative insertion of Pd is lower than that for S_N2 substitution. The activation strain diagram in Fig. 7 shows that this is due to a more favorable interaction in the OxIn pathway which derives from a better overlap between the metal-*d* and substrate $\sigma^*_{C\text{-}X}$ orbitals in the side-on approach, as compared to the back-side approach of the S_N2 pathway.[12,34] Note also that this causes the S_N2 transition state to occur later, at a point where there is significantly more C–Cl stretch.

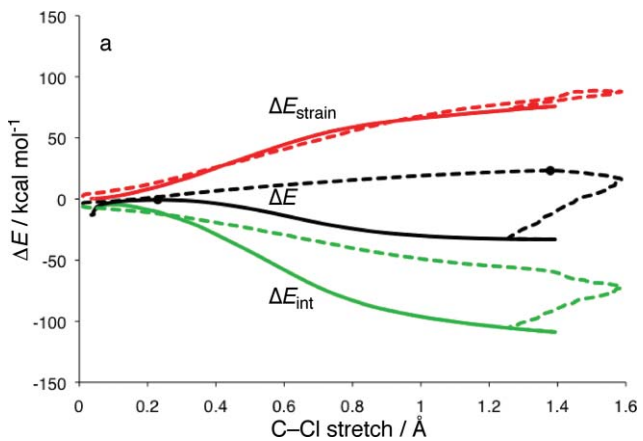

Fig. 7 Activation strain analyses for palladium-induced chloromethane C–Cl bond activation *via* oxidative insertion (solid lines) and S_N2 substitution (dashed lines).

Interestingly, anion assistance can shift the reactivity towards the S_N2 pathway.[34] The reason for this inversion in relative reactivity is the aforementioned strengthening of the interaction energy ΔE_{int} that occurs as the Cl^- ligand is coordinated to palladium. This lowers the barriers of both pathways. But the S_N2 pathway "benefits" most because its transition state occurs later along the reaction coordinate, at a point where the ΔE_{int} term and, thus, also its strengthening due to anion assistance are larger.

Solvation has opposite effects on the neutral and anion-assisted reactions, which can be understood with an activation strain model that has been extended to incorporate solvent effects.[34] Thus, solvation shifts oxidative addition to Pd from the OxIn towards the S_N2 pathway, among others, because it induces a stronger charge separation across the C–X bond and, thus, a stronger interaction ΔE_{int}. And, as pointed out above, the S_N2 pathway benefits most from a strengthening in the interaction term.

On the other hand, solvation on top of anion assistance shifts the reactivity back, from S_N2 to OxIn. The interaction term ΔE_{int} is again responsible. This time, the dominant solvent effect is a stabilization of the charged catalyst complex $PdCl^-$ and a lowering of the energy of its metal *d*-derived frontier orbitals. This diminishes the bonding capabilities of the model catalyst and therefore reduces the stabilizing catalyst–substrate interaction. Again, the S_N2 pathway is most affected by this change in ΔE_{int} which, this time, however, comes down to a destabilization.

4. S_N2 reactions

Nucleophilic substitution (S_N2, see Scheme 6) plays an important role in many areas of chemistry: organic, inorganic and biological. Our group has studied various aspects of this class of reactions, covering nucleophilicity of X^-, leaving-group ability of Y, role of the electrophilic center A, effect of substituents R as well as solvent effects.[45–48] Activation strain analyses[45] reveal that the central barrier of nucleophilic substitution at carbon (S_N2@C) is steric in nature:[46] it arises from the steric congestion that occurs in the S_N2 transition state in which five substituents try to approach the relatively small carbon atom. The steric (Pauli) repulsion that occurs between these five substituents as the nucleophile X^- approaches causes deformations in the substrate CR_3Y: the C–R bonds bend away from the approaching nucleophile and the C–Y bond elongates. The geometrical deformation induced by steric interactions shows up in a relatively high strain energy ΔE_{int}. Note that the geometrical deformations in the S_N2 transition state relieve and therefore mask the steric repulsion which caused them in the first place.[45] In other words, the steric (Pauli) repulsion that would otherwise occur in the interaction ΔE_{int} between the reactants, is transformed into strain energy ΔE_{strain} within the reactants. This phenomenon, *i.e.*, geometrical relaxation processes that relieve

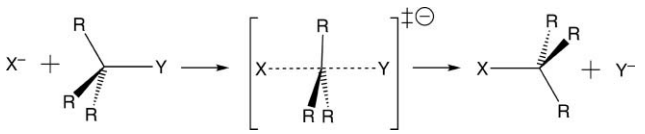

Scheme 6 S_N2 reaction.

and thus hide the (steric) interactions by which they are induced, occurs more generally in chemistry but it is often overlooked.[47]

The steric congestion in the S_N2 transition state decreases drastically if one goes from substitution at the small carbon atom, *e.g.*, in $Cl^- + CH_3Cl$ (S_N2@C), to substitution at the larger silicon atom, *e.g.*, in $Cl^- + SiH_3Cl$ (S_N2@Si), which allows for more space between the five substituents in the five-coordinate transition state.[45] Consequently, the strain curve drops and the central barrier disappears, turning the five-coordinate transition species into a stable complex in the case of silicon as the central atom ("transition complex"). Interestingly, the "carbon behavior", which is characterized by substitution proceeding *via* a central barrier, reappears as the steric bulk around the silicon atom and thus the strain curve ΔE_{strain} is raised along the model reactions $Cl^- + SiH_3Cl$, $Si(CH_3)_3Cl$ and $Si(OCH_3)_3Cl$.[45b] This further consolidates the steric nature of the S_N2 barrier in general.

At this point we stress that the height of the S_N2 barrier also strongly depends on electronic effects, such as the mutual bonding capabilities of the reactants as well as their internal bonding or rigidity.[45,48] Activation strain analyses of halides reacting with halomethanes show that nucleophilicity directly and straightforwardly depends on the electron donating capability of the nucleophile:[48] a higher-energy n*p* atomic orbital on the halide X^- causes more stabilizing interactions ΔE_{int} with the substrate and thus a lower S_N2 barrier (see Fig. 8a). On the other hand, a stronger carbon–leaving-group (C–Y) bond translates directly into a more destabilizing strain curve ΔE_{strain} and therefore a higher S_N2 barrier (see Fig. 8b).

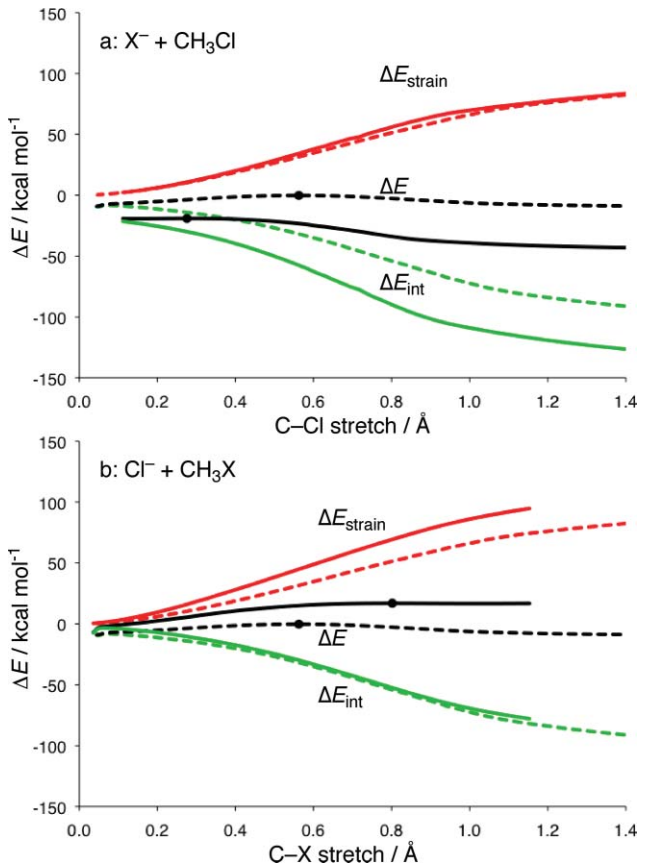

Fig. 8 Activation strain analysis for S_N2 reactions of (a) $X^- + CH_3Cl$ (variation of nucleophile) and (b) $Cl^- + CH_3X$ (variation of leaving group) with X = F (solid lines) and Cl (dashed lines).[48]

The fact that S_N2 proceeds in general *via* a backside attack and inversion of configuration (Walden inversion) and not *via* a frontside attack (which would go with retention of configuration) is mainly due to the higher steric congestion in the frontside transition state in which the nucleophile and leaving-group are in close proximity (see Scheme 7).[48] This situation leads to more deformation which is reflected by a higher strain ΔE_{strain}. Frontside attack also suffers from a smaller overlap between the n*p* atomic orbital on the halide nucleophile X^- and the substrate σ^*_{C-Y} acceptor orbital if compared to the situation for backside attack. However, this overlap effect and the associated weakening in the interaction term are less important for the preference of backside over frontside S_N2 substitution than the steric crowding in the latter transition state mentioned above. Similar findings were reported for S_N2 substitution at heavier group-14 atoms[45c] and at disulfides.[49]

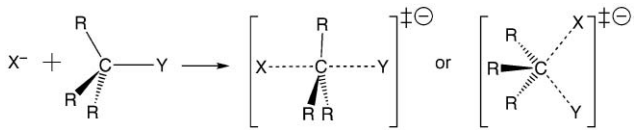

Scheme 7 Backside and frontside S_N2 transition states.

Sung *et al.* found that halide and amine substitutions at sulfonyl centers benefit greatly from the positively charged sulfur in the sulfonyl group which leads to a substantially more stabilizing nucleophile–substrate interaction than in the case of substitution at carbon.[50]

The origin of the S_N2 benzylic effect was uncovered by Allen and coworkers using, among others, detailed activation strain analyses.[51] The critical effect of the aromatic ring in benzylic S_N2 systems is to raise the electrostatic potential near the electrophilic carbon atom which shows up in a more stabilizing nucleophile–substrate interaction ΔE_{int}. Fábián *et al.* used an activation strain analysis to show that substitution with pyridine at phenacyl bromides proceeds with lower barriers than at 2-phenylethyl-bromides, due to a more stabilizing interaction caused by the π^* acceptor orbital at the carbonyl group of phenacyl.[52]

Recently, Wu *et al.* explored the competition between S_N2 and E2 pathways for a range of anionic bases reacting with ethyl chloride.[53] They consolidated earlier findings[9] that the E2 pathway, despite having a more distortive character and higher activation strain $\Delta E^{\ddagger}_{strain}$, dominates the S_N2 pathway in the gas phase because of a more stabilizing TS interaction $\Delta E^{\ddagger}_{int}$. Yun *et al.* rationalized the preference of hydride attacks on different positions on aziridinium ions *via* differences in distortion energies in the transition states, related to the relative amount of stretch of the carbon–leaving-group bond in the transition states.[54]

5. Pericyclic reactions

The Houk group has opened up the field of studying pericyclic reactions using the activation strain model (or distortion/interaction model), with an investigation of 1,3-dipolar cycloadditions of compounds of the type $X–Y^+–Z^-$ with ethylene or acetylene (see Scheme 8).[55] They found that the activation

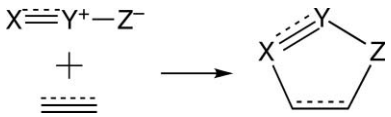

Scheme 8 1,3-dipolar cycloaddition.

energy of 1,3-dipolar additions is determined by (and follows the trend of) the activation strain which is dictated mainly by the bending of the 1,3-dipole. Only when the strain energies within a set of reactants remain similar, does the change in orbital interactions (which contribute *via* ΔE_{int}) become large enough to modulate the trend in reactivity. In a very recent study on 1,3-dipolar additions, the activation strain model has been connected with the dynamics involved in these reactions.[56] It was shown that, in order for certain 1,3-dipolar cycloadditions to proceed, the dipole bending mode which also features in the decisive activation strain term, must be vibrationally excited.

Ess has expanded the above work to the addition of MO_4 complexes to ethane, a reaction which can proceed *via* a comparable mechanism.[57] His findings show that activity differences for OsO_4, ReO_4^-, TcO_4^-, and MnO_4^- are mainly due to changes in electron transfer, while the strain terms change little. In related work, Schoenebeck *et al.* investigated the effect of using cycloalkynes and cycloalkenes as substrates for 1,3 dipolar cycloaddition.[58] In general, a smaller ring size in these reactions will lead to a less destabilizing distortion energy in the transition state due to the strained nature of the ring. The group of Houk has also investigated Diels–Alder reactions, employing the activation strain model to gain insight into the role of distortion in the reactants in connection with the precise nature of the reaction mechanism and trends in reactivity.[59,60]

Fernández *et al.* recently applied the activation strain model to double group transfer (DGT) reactions, a type of pericyclic reaction in which two groups, here, two hydrogens, migrate in a concerted manner from a donor to an acceptor fragment (see Scheme 9).[61] The strain appears to be again the controlling factor for the high activation barrier in these DGT reactions, similar to the situation found by Houk for 1,3-dipolar additions. The high activation strain in DGT reactions explains why these processes occur with high barriers despite the fact the transition state is in-plane aromatic, *i.e.*, it receives stabilization from cyclic 6-electron conjugation.

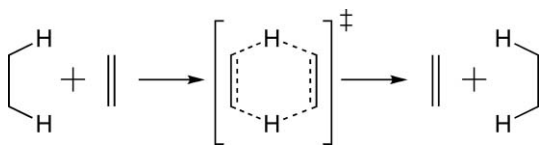

Scheme 9 Double group transfer (DGT) reaction.

6. Conclusions

In various applications, we have shown here how the activation strain model provides qualitative insight, based on accurate calculations, into the origin of reaction barriers and especially trends therein, in terms of the properties of the reactants. In this model, the reaction energy profile ΔE along the reaction coordinate ζ is decomposed into strain (or deformation) energy of the reactants, ΔE_{strain}, plus the mutual interaction energy between the reactants: $\Delta E(\zeta) = \Delta E_{strain}(\zeta) + \Delta E_{int}(\zeta)$.

The strain is directly related to not only the rigidity of the reactants (*i.e.*, bonding within the individual reactants) but also to the extent of distortion that is characteristic for a particular type of reaction mechanism. The interaction reflects the bonding capabilities of the reactants, that is, their ability to enter into electrostatic or donor–acceptor (for example, HOMO–LUMO) orbital interactions.

The insight that evolves from activation strain analyses can be used to *a posteriori* interpret and rationalize computational (and experimental!) findings. Importantly, the emerging concepts can also guide a more rational optimization or design of new reactions (*e.g.*, catalyst design).

Acknowledgements

We thank the National Research School of Combination-Catalysis (NRSC-C) and The Netherlands Organization for Scientific Research (NWO-CW) for financial support.

Notes and references

1 R. B. Woodward and R. Hoffmann, *J. Am. Chem. Soc.*, 1965, **87**, 395–397.
2 R. Hoffmann, *J. Chem. Phys.*, 1963, **39**, 1397–1412.
3 T. A. Albright, J. K. Burdett and M.-H. Whangbo, *Orbital interactions in chemistry*, Wiley-Interscience, New York, 1985.
4 M. J. S. Dewar, *Angew. Chem., Int. Ed. Engl.*, 1971, **10**, 761–776.
5 I. Flemming, *Frontier orbitals and organic chemical reactions*, Wiley, New York, 1976.
6 S. S. Shaik, P. C. Hiberty, *A Chemist's Guide to Valence Bond Theory*, Wiley-Interscience, Hoboken, New Jersey, 2007.
7 R. A. Marcus, *Annu. Rev. Phys. Chem.*, 1964, **15**, 155–196.
8 See, for example: J. P. Guthrie, *ChemPhysChem*, 2003, **4**, 809–816.
9 (*a*) F. M. Bickelhaupt, *J. Comput. Chem.*, 1999, **20**, 114–128. Other studies in which the reactant strain or distortion energy have been separated from the interaction energy for understanding chemical reactions are, for example: (*b*) D. J. Mitchell, H. B. Schlegel, S. S. Shaik and S. Wolfe, *Can. J. Chem.*, 1985, **63**, 1642; (*c*) C. Y. Legault, Y. Garcia, C. A. Merlic and K. N. Houk, *J. Am. Chem. Soc.*, 2007, **129**, 12664.
10 A. Diefenbach, G. T. de Jong and F. M. Bickelhaupt, *Mol. Phys.*, 2005, **103**, 995–998.
11 J. N. P. van Stralen and F. M. Bickelhaupt, *Organometallics*, 2006, **25**, 4260–4268.
12 G. T. de Jong and F. M. Bickelhaupt, *ChemPhysChem*, 2007, **8**, 1170–1181.
13 W. J. van Zeist, A. H. Koers, L. P. Wolters and F. M. Bickelhaupt, *J. Chem. Theory Comput.*, 2008, **4**, 920–928.
14 F. M. Bickelhaupt, and E. J. Baerends, in *Reviews in Computational Chemistry*, ed. K. B. Lipkowitz, and D. B. Boyd, VCH Publishers Inc., New York, 2000, pp. 1–86.
15 E. J. Baerends and O. V. Gritsenko, *J. Phys. Chem. A*, 1997, **101**, 5383–5403.
16 T. Ziegler and A. Rauk, *Inorg. Chem.*, 1979, **18**, 1558–1565.
17 K. Ishida, K. Morokuma and A. Komornicki, *J. Chem. Phys.*, 1977, **66**, 2153–2156.
18 C. Gonzalez and H. Schlegel, *J. Phys. Chem.*, 1990, **94**, 5523–5527.
19 K. Fukui, *Acc. Chem. Res.*, 1981, **14**, 363–369.
20 K. Fukui, *J. Phys. Chem.*, 1970, **74**, 4161–4163.
21 W. J. van Zeist, C. Fonseca Guerra and F. M. Bickelhaupt, *J. Comput. Chem.*, 2008, **29**, 312–315.
22 (*a*) See for example: W. J. van Zeist and F. M. Bickelhaupt, *Phys. Chem. Chem. Phys.*, 2009, **11**, 10317–10322; (*b*) A. Krapp, F. M. Bickelhaupt and G. Frenking, *Chem.–Eur. J.*, 2006, **12**, 9196–9216.
23 F. M. Bickelhaupt and E. J. Baerends, *Angew. Chem., Int. Ed.*, 2003, **42**, 4183–4188.

24 J. Poater, M. Solà and F. M. Bickelhaupt, *Chem.–Eur. J.*, 2006, **12**, 2889–2895.
25 (*a*) J. P. Collman, L. S. Hegedus, J. R. Norton, and R. G. Finke, *Principles and Applications of Organotransition Metal Chemistry*, University Science Books, Mill Valley, California, 1987; (*b*) M. B. Smith, and J. March, *March's Advanced Organic Chemistry*, 6th ed., Wiley-Interscience, New York, 2007; (*c*) C. A. Elschenbroich, *Organometallics*, Wiley-VCH, Weinheim, 2006.
26 K. C. Nicolaou, P. G. Bulger and D. Sarlah, *Angew. Chem.*, 2005, **117**, 4516–4563.
27 (*a*) A. Dedieu, *Chem. Rev.*, 2000, **100**, 543–600; (*b*) L. Xue and Z. Lin, *Chem. Soc. Rev.*, 2010, **39**, 1692–1705; (*c*) C. J. Cramer and D. G. Truhlar, *Phys. Chem. Chem. Phys.*, 2009, **11**, 10757–10816.
28 A. Diefenbach and F. M. Bickelhaupt, *J. Chem. Phys.*, 2001, **115**, 4030–4040.
29 A. Diefenbach and F. M. Bickelhaupt, *J. Phys. Chem. A*, 2004, **108**, 8460–8466.
30 A. Diefenbach, G. T. de Jong and F. M. Bickelhaupt, *Mol. Phys.*, 2005, **103**, 995–998.
31 A. Diefenbach, G. T. de Jong and F. M. Bickelhaupt, *J. Chem. Theory Comput.*, 2005, **1**, 286–298.
32 G. T. de Jong, R. Visser and F. M. Bickelhaupt, *J. Organomet. Chem.*, 2006, **691**, 4341–4349.
33 G. T. de Jong and F. M. Bickelhaupt, *J. Chem. Theory Comput.*, 2006, **2**, 322–335.
34 G. T. de Jong and F. M. Bickelhaupt, *J. Chem. Theory Comput.*, 2007, **3**, 514–529.
35 W. J. van Zeist, R. Visser and F. M. Bickelhaupt, *Chem.–Eur. J.*, 2009, **15**, 6112–6115.
36 J. J. Low and W. A. Goddard III, *Organometallics*, 1986, **5**, 609–622.
37 P. E. M. Siegbahn and M. R. A. Blomberg, *J. Am. Chem. Soc.*, 1992, **114**, 10548–10556.
38 C. Y. Legault, Y. Garcia, C. A. Merlic and K. N. Houk, *J. Am. Chem. Soc.*, 2007, **129**, 12664–12665.
39 S. I. Gorelsky, D. Lapointe and K. Fagnou, *J. Am. Chem. Soc.*, 2008, **130**, 10848–10849.
40 D. H. Ess, S. M. Bischof, J. Oxgaard, R. A. Periana and W. A. Goddard, *Organometallics*, 2008, **27**, 6440–6445.
41 A. Ariafard and Z. Lin, *Organometallics*, 2006, **25**, 4030–4033.
42 R. Fazaeli, A. Ariafard, S. Jamshidi, E. S. Tabatabaie and K. A. Pishro, *J. Organomet. Chem.*, 2007, **692**, 3984–3993.
43 A. Ariafard and B. F. Yates, *J. Organomet. Chem.*, 2009, **694**, 2075–2084.
44 G. T. de Jong and F. M. Bickelhaupt, *Can. J. Chem.*, 2009, **87**, 806–817.
45 (*a*) M. A. van Bochove, M. Swart and F. M. Bickelhaupt, *J. Am. Chem. Soc.*, 2006, **128**, 10738–10744; (*b*) A. P. Bento and F. M. Bickelhaupt, *J. Org. Chem.*, 2007, **72**, 2201–2207; (*c*) A. P. Bento and F. M. Bickelhaupt, *Chem.–Asian J.*, 2008, **3**, 1783–1792.
46 Alternative perspectives on the steric nature of the S_N2 barriers: (*a*) S. C. A. H. Pierrefixe, S. J. M. van Stralen, J. N. P. van Stralen, C. Fonseca Guerra and F. M. Bickelhaupt, *Angew. Chem., Int. Ed.*, 2009, **48**, 6469–6471; (*b*) S. C. A. H. Pierrefixe, J. Poater, C. Im and F. M. Bickelhaupt, *Chem.–Eur. J.*, 2008, **14**, 6901–6911; (*c*) S. C. A. H. Pierrefixe, C. Fonseca Guerra and F. M. Bickelhaupt, *Chem.–Eur. J.*, 2008, **14**, 819–828.
47 (*a*) See, for example: S.-G. Wang, Y.-X. Qiu and W. H. E. Schwarz, *Chem.–Eur. J.*, 2009, **15**, 6032–6040; (*b*) J. Poater, R. Visser, M. Solà and F. M. Bickelhaupt, *J. Org. Chem.*, 2007, **72**, 1134–1142.
48 A. P. Bento and F. M. Bickelhaupt, *J. Org. Chem.*, 2008, **73**, 7290–7299.
49 (*a*) E. H. Krenske, W. A. Pryor and K. N. Houk, *J. Org. Chem.*, 2009, **74**, 5356–5360; (*b*) R. D. Bach, O. Dmitrenko and C. Thorpe, *J. Org. Chem.*, 2008, **73**, 12–21; (*c*) A. T. P. Carvalho, M. Swart, J. N. P. van Stralen, P. A. Fernandes, M. J. Ramos and F. M. Bickelhaupt, *J. Phys. Chem. B*, 2008, **112**, 2511–2523; (*d*) J. M. Hayes and S. M. Bachrach, *J. Phys. Chem. A*, 2003, **107**, 7952–7961.
50 D. D. Sung, T. J. Kim and I. Lee, *J. Phys. Chem. A*, 2009, **113**, 7073–7079.
51 B. Galabov, V. Nikolova, J. J. Wilke, H. F. Schaefer and W. D. Allen, *J. Am. Chem. Soc.*, 2008, **130**, 9887–9896.
52 A. Fábián, F. Ruff and Ö. Farkas, *J. Phys. Org. Chem.*, 2008, **21**, 988–996.
53 X.-P. Wu, X.-M. Sun, X.-G. Wei, Y. Ren, N.-B. Wong and W.-K. Li, *J. Chem. Theory Comput.*, 2009, **5**, 1597–1606.
54 S. Y. Yun, S. Catak, W. K. Lee, M. D'hooghe, N. De Kimpe, V. Van Speybroeck, M. Waroquier, Y. Kim and H.-J. Ha, *Chem. Commun.*, 2009, 2508–2510.
55 See, for example: D. H. Ess and K. N. Houk, *J. Am. Chem. Soc.*, 2008, **130**, 10187–10198.
56 L. Xu, C. E. Doubleday and K. N. Houk, *Angew. Chem., Int. Ed.*, 2009, **48**, 2746–2748.
57 D. H. Ess, *J. Org. Chem.*, 2009, **74**, 1498–1508.
58 F. Schoenebeck, D. H. Ess, G. O. Jones and K. N. Houk, *J. Am. Chem. Soc.*, 2009, **131**, 8121–8133.
59 Y.-H. Lam, P. H.-Y. Cheong, J. M. Blasco Mata, S. J. Stanway, V. r. Gouverneur and K. N. Houk, *J. Am. Chem. Soc.*, 2009, **131**, 1947–1957.
60 A. E. Hayden and K. N. Houk, *J. Am. Chem. Soc.*, 2009, **131**, 4084–4089.
61 I. Fernández, F. M. Bickelhaupt and F. P. Cossio, *Chem.–Eur. J.*, 2009, **15**, 13022–13032.